Intercomparison of Heat Fluxes in the South Atlantic. Part I: The Seasonal Cycle

ILANA WAINER AND ANDREA TASCHETTO

Department of Physical Oceanography, University of São Paulo, São Paulo, Brazil

JACYRA SOARES AND AMAURI PEREIRA DE OLIVEIRA

Department of Atmospheric Sciences, University of São Paulo, São Paulo, Brazil

BETTE OTTO-BLIESNER AND ESTHER BRADY

National Center for Atmospheric Research, Boulder, Colorado

(Manuscript received 28 September 2001, in final form 4 March 2002)

ABSTRACT

Intercomparison of the seasonal cycle for the fluxes of sensible and latent heat for four observation-based products [DaSilva, NCEP, Esbensen–Kushnir (EK), and the Southampton Oceanography Centre (SOC)] and the results for the NCAR Community Climate System Model (CCSM) are examined in order to gain an improved understanding of the South Atlantic characteristic spatial patterns. Their seasonal structure associated with ocean dynamics, evolution, and the net heat flux patterns are also discussed.

The key regions of the Brazil–Malvinas confluence, Agulhas retroflection, and Benguela upwelling region off Africa were chosen for a closer examination of the fluxes. All climatologies show very different behavior. The SOC product presents sudden changes in the seasonal cycle evolution, departing from the annual or semiannual observed pattern of EK and NCEP. Compared to the other climatologies, EK shows equivalent temporal behavior but different magnitudes because this climatology covers a period where much less data was available.

It was found that the eastern Atlantic shows more differences among the climatologies than the Brazil–Malvinas confluence region in the west. It is also in the eastern Atlantic that the difference between NCAR CCSM results and observations are bigger, probably due to a bias in cloud simulation, which affects the air–sea interaction dynamics. In the Brazil–Malvinas confluence region differences between the NCAR CCSM and the observed datasets are comparable to the difference between the observations themselves.

1. Introduction

Many ocean properties show strong links to overlying atmospheric variability, suggesting that much of the observed ocean variability is driven by the atmosphere. In the tropical Atlantic, sea surface temperature variability and associated changes in the intertropical convergence zone and the Hadley circulation occur on interannual to decadal timescales, phenomena known as the interhemispheric SST gradients (the so-called dipole). While it is known that the dipole plays a central role in modulating climate, its interaction with the southern part of the basin is less known. Furthermore ocean and atmospheric variability on interannual to decadal timescales in the South Atlantic is less clear. Some progress has been made both in terms of our understanding of the South Atlantic and our ability to observe them but much remains to be uncovered, in particular with respect to the sensitivity of the South Atlantic to climate change scenarios.

Variations of the South Atlantic Ocean circulation patterns and SST can occur over timescales ranging from subseasonal to the seasonal and interannual. These variations are strongly influenced by interactions between the Brazil Current and the Malvinas Current, which in turn are affected by the basin-scale wind field and other atmospheric features (Campos et al. 1999).

The most dramatic contrasts in SST of the entire South Atlantic occur at its western boundary where warm and salty waters of the southward-flowing Brazil Current meet the colder and fresher waters of the northward-flowing Malvinas Current [Fig. 1 from Olson et al. (1988)], where temperature gradients are as high as 1°C (100 m)$^{-1}$ (Campos et al. 1999). A schematic of the currents can be seen in Fig. 1.

The confluence zone between these two currents migrates up and down the continental margin at seasonal, interannual, and possibly longer timescales, affecting the cyclogenesis frequency and the regional rainfall dis-

Corresponding author address: Dr. Ilana Wainer, Department of Physical Oceanography, University of São Paulo, Praca do Oceanografico 191, São Paulo, SP 05508-900 Brazil.
E-mail: wainer@usp.br

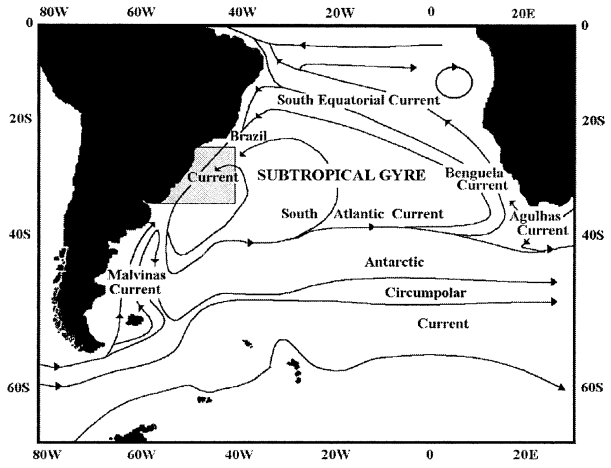

FIG. 1. Schematic figure of the South Atlantic currents adapted from (Zavialov et al. 1999).

tribution. Indeed, the links between SST anomalies in the southwestern Atlantic Ocean and rainfall anomalies in the entire region are more pronounced during October–December and April–July (Diaz et al. 1998). The fact that the years that show more rain than the expected climatological value do not necessarily coincide with El Niño–Southern Oscillation (ENSO) years, indicates that the SST anomalies in the Atlantic may contribute on their own way to the rainfall anomalies over Uruguay and southern Brazil.

Although there is significant evidence showing the importance of monitoring South Atlantic SST anomalies for regional climate and weather prediction in southern South America, much work is still needed in order to understand the details of how these SST anomalies (sometimes short lived) affect rainfall regimes, weather patterns, and how (or if) these in turn will modify the SST distribution.

The region of this study lies between the equator and 55°S and between 65°W and 20°E encompassing to the west the Brazil–Malvinas confluence (BMC). The confluence region, one of the most energetic areas of the World Ocean (Chelton et al. 1990) is characterized by strong thermohaline gradients and intense mesoscale activity (Gordon 1988; Cheney et al. 1983). Typically at about 38°S, the Brazil Current separates from the coast and veers offshore together with the Malvinas Current. The latitude of separation exhibits strong seasonal and interannual variations (Olson et al. 1988).

Also important is the Agulhas Current retroflection region, in the southeast edge of the region of interest (Lutjeharms and van Ballegooyen 1988). The Agulhas Current flows along the east coast of South Africa in the Indian Ocean and plays an important role in ocean heat transport. In the vicinity of the Cape of Good Hope, the Agulhas Current encounters the eastward flow of the Antarctic Circumpolar Current and the northeastward flow of the Benguela Current and retroflects producing a turbulent zone of mixing (Olson and Evans 1986). Rings formed in the Agulhas retroflection have been observed in the southern Atlantic and can migrate to the South American coast transporting enormous amounts of heat, salt, and momentum into the Atlantic Ocean. This interocean exchange is one of the major links in the global thermohaline circulation.

Finally, another important feature of the South Atlantic Ocean is the Benguela upwelling region located near the strong Benguela Current. This current is cold, and originates in the Southern Ocean flowing from south to north along the South African and Namibian coastline. The Benguela Current is a classic eastern ocean coastal upwelling system along southwestern Africa.

Major uncertainties remain in the understanding of the fundamental processes of air–sea interaction in the South Atlantic. There are very few studies in this region that directly consider the variability of the ocean–atmospheric fluxes. However, it is through the exchange of heat, moisture, and momentum that the atmosphere interacts with the ocean. Thus, it is not the SST itself, but these energy fluxes to and from the ocean that actually force the atmospheric circulation and, at the same time, control the ocean temperature. Understanding the coupled ocean–atmosphere system depends largely on the scales of interaction between the two fluids and the processes that provide the strongest feedbacks.

In this work, we examine the seasonal cycle of SST from three observation-based products [DaSilva, the National Centers for Environmental Prediction (NCEP) and Esbensen–Kushnir (EK)] and the coupled model results for the National Center for Atmospheric Research (NCAR) Community Climate System Model (CCSM). We also examine and compare the seasonal cycle for sensible, latent, and net heat fluxes available from four observation-based products [DaSilva, NCEP, EK, and the Southampton Oceanography Centre (SOC)] and the coupled model results for the NCAR CCSM in order to gain an improved understanding of the characteristic South Atlantic spatial patterns, their seasonal structure, and how they evolve.

2. Data

Subsets for the South Atlantic are obtained from the following data products:

- DaSilva [1945–93 climatology (DaSilva et al. 1994)]: This dataset is based on Comprehensive Ocean–Atmosphere Data Set (COADS), but has improved resolution ($1° \times 1°$) and boundary layer parameterizations, and includes a new scientific Beaufort equivalent scale, which reduces wind speed bias and artificial wind speed trends.
- NCEP [NCEP–NCAR reanalysis project (Kalnay et al. 1986)]: The goal of this joint effort is to produce new atmospheric analyses using historical data (1957 onward) and as well to produce analyses of the current

TABLE 1. Characteristics of the observed climatological air–sea flux datasets used in this study: SW and LW are shortwave and longwave radiation terms, respectively; *H* is the sensible heat; LE is the latent heat; and WS is the wind scale [adapted from Taylor (2000)].

Dataset	Area	Period	Grid (lat–lon)	SW	LW	*H*-LE	WS
EK (Esbensen and Kushnir 1981)	Globe	1946–79	4° × 5°	Budyko (1963)	Berliand and Berliand (1952)	Liu et al. (1979)	WMO 1100
DaSilva et al., 1994	Globe	1945–89	1° × 1°	Reed (1977)	Rosati and Miyakoda (1988)	Large and Pond (1982)	DaSilva et al. (1994)
SOC (Josey et al., 1999)	Globe	1980–93	1° × 1°	Reed (1977)	Clark et al. (1974)	Smith (1988)	Lindau (1995)

atmospheric state [Climate Data Assimilation System, (CDAS)]. The climatology analyzed covers the period from 1957 to 1996 at 2.5° × 2.5° resolution.

- EK [Esbensen–Kushnir monthly climatologies archived at NCAR (Esbensen and Kushnir 1981)]: Global ocean radiation and heat budget data are prepared on a 4° × 5° lat–lon grid covering the period from 1946 to 1979.
- SOC [Southampton Oceanography Centre (Josey et al. 1999) climatology]: The 1° × 1° dataset was obtained from in situ reports within COADS 1a, a global dataset containing about 30 million surface observations from ships and buoys collected over the period 1980–93. Additional information about measurement procedures has been blended in from the World Meteorological Organization (WMO 1970) list of ships and used to correct the flux variables.
- NCAR CCSM [Paleoclimate Comunity Climate System Model results for present-day levels of trace and greenhouse gases (Boville and Gent 1998)]: The NCAR CCSM is a global general circulation model that couples the atmosphere and ocean and includes land and sea ice components. It was developed at NCAR. The resolution of the ocean model is 2° × 2°. The model output is monthly mean data from 150 years of the NCAR CCSM run (Wainer et al. 2000). The control run—no trace or greenhouse gases—shows negligible trends in SST and sea level pressure. No flux adjustment is used throughout the integrations.

Table 1 summarizes the characteristics of the *observed* climatological air–sea flux datasets used in this study. It should be noted that that the fluxes from these datasets are not directly observed, but rather calculated using bulk formulas. The algorithms and exchange coefficient for each of the products are different. More specific details and a comprehensive discussion of the flux products are given in the (Taylor 2000) report on ocean fluxes.

Energy exchange between the atmosphere and ocean

Interaction of the atmosphere and the ocean is based on the exchange of matter, energy, and momentum across the sea surface, involving both turbulent and laminar processes modified by wave breaking, surface tension, the structure of the planetary boundary layer and the ocean mixed layer, and other effects.

The net heat flux (Q_{net}) is an important component of ocean–atmosphere interactions. It can be obtained integrating the energy conservation law in the ocean, considering the lateral and bottom boundary fluxes null:

$$Q_{\text{net}} = \frac{1}{S}\int_V oc_v \frac{dT}{dt}\, dV = \frac{1}{S}\int_S (H_0 + \text{LE}_0 + \text{RN}_0)\, dS, \quad (1)$$

where H_0 is the sensible heat flux, LE_0 is latent heat flux, and RN_0 is the net radiation at the ocean surface; ρ is sea density; c_v is the sea specific heat at constant volume; T is the sea temperature; S and V are the domain area and volume, respectively. By convention, the heat gain for the ocean is positive and the heat loss is negative.

Most of the large-scale applications of the surface turbulent fluxes are based on bulk formula parameterizations, with the fluxes being a function of the surface layer mean wind and of the thermal and moisture atmospheric contrasts induced by the ocean (Bèranger et al. 1999):

$$H_0 = -\rho_0 c_p C_H U_r(\text{SST} - T_r) \quad (2)$$

$$\text{LE}_0 = -\rho_0 L C_E U_r(q_s - q_r), \quad (3)$$

where ρ_0 is the air density; c_p is the air specific heat at constant pressure; C_H is the heat exchange coefficient; U_r is the wind velocity at the reference level; T_r is the air temperature at the reference level; L is the latent heat of evaporation; C_E is the moisture exchange coefficient; q_s is the saturation specific humidity at the surface; q_r is the air specific humidity at the reference level; and c_v is the air specific heat at a constant volume.

The net radiation flux at the ocean surface is evaluated considering the shortwave (SW) and longwave (LW) atmospheric components at the air–sea interface:

$$\text{RN}_0 = \text{LW}_{\text{up}} + \text{LW}_{\text{down}} + \text{SW}_{\text{up}} + \text{SW}_{\text{down}}. \quad (4)$$

The net heat flux [Eq. (1)] is the sum of the radiation flux components [Eq. (4)] plus the turbulent flux com-

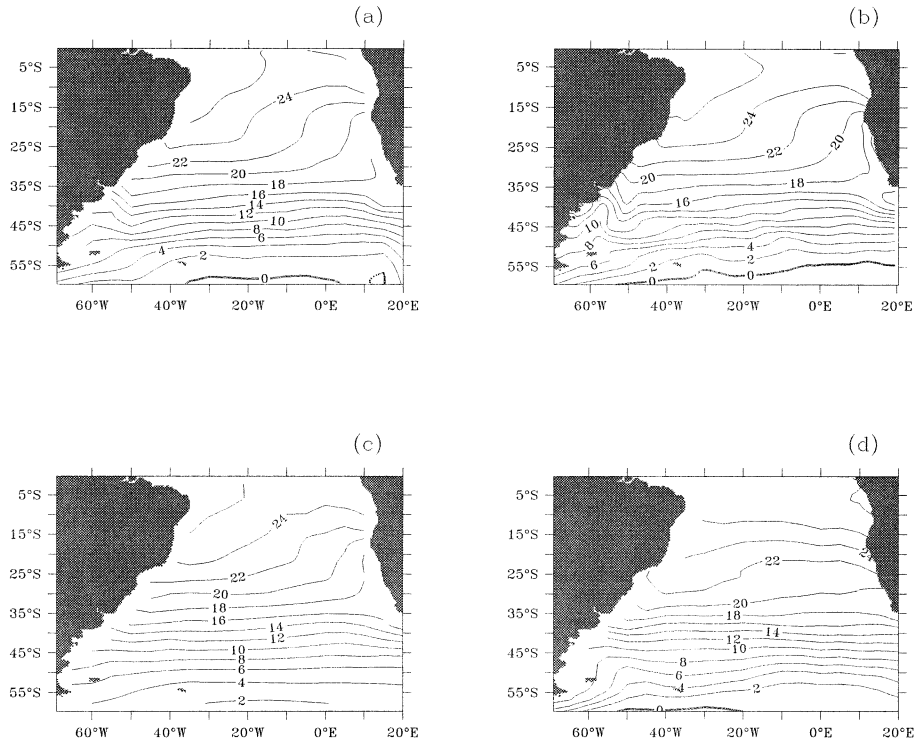

FIG. 2. South Atlantic SST (°C) annual mean climatology for (a) DaSilva, (b) NCEP, (c) EK, and (d) NCAR CCSM model output. Contour interval is 2 °C.

ponents [Eqs. (2) and (3)]. Here, the ocean loses energy when evaporation occurs and when the sensible heat flux is positive.

3. Results

Annual, seasonal, and monthly mean climatologies are intercompared.

a. Annual means

Annual averages of SST, latent, and net heat fluxes are presented in Figs. 2–4.

Poleward of 35°S all climatologies show an intensification of the meridional gradient in SST (Figs. 2a–d). Differences between the climatologies are prominent near the South American coast, in the BMC region (40°S, 50°W) where the associated SST front is barely visible in the DaSilva dataset (Fig. 2a) and NCAR CCSM model output (Fig. 2d), nonexistent in EK (Fig. 2c), but well represented in NCEP (Fig. 2b). With the exception of the NCAR CCSM (Fig. 2d) all climatologies show a upwelling region off the southwest coast of Africa, centered at approximately 27°S. The smallest differences were found between the DaSilva (Fig. 2a) and NCEP (Fig. 2b) climatologies, just 0.5°C off the southwest African coast and 2°C in the vicinity of the BMC region. The largest differences in the annual mean are found between the NCEP (Fig. 2b) and EK (Fig. 2c) products, with a 5°C difference in the BMC region, and about a 4°C difference in the Agulhas Current retroflection region (40°S, 10°E).

Latent heat flux (Fig. 3) in the South Atlantic is characterized by a region of greater loss in the central western part of the basin, well within the southeast trade wind system, around 10°S, reaching values of at least -120 W m^{-2}. In this region the maximum latent heat loss of 160 W m^{-2} is found in the NCEP dataset (Fig. 3b). Differences between the observed data products and the modeled latent heat flux (Fig. 3e) are more prominent off the southwest coast of Africa, in the Benguela Current, reaching as much as -80 W m^{-2} when compared to the SOC climatology. Compared to the SOC climatology, the BMC region shows differences of the order of 40 W m^{-2} with respect to the NCAR CCSM. This indicates that, in general, there is an excessive loss of latent heat flux in the NCAR CCSM in all of the South Atlantic with the exception of the BMC region.

Around the Benguela Current upwelling system (10°S, 10°E) and in the BMC region (40°S, 50°W) the relative minimum latent heat loss seems to be connected to the flow of cold waters. Off the southern coast of Africa, in the Benguela Current system, there is a predominance of the meridional component of the wind stress inducing coastal upwelling. In the BMC region it is the cold Malvinas Current that gains heat as it flows northward.

Sensible heat flux (not shown) contributes only a mi-

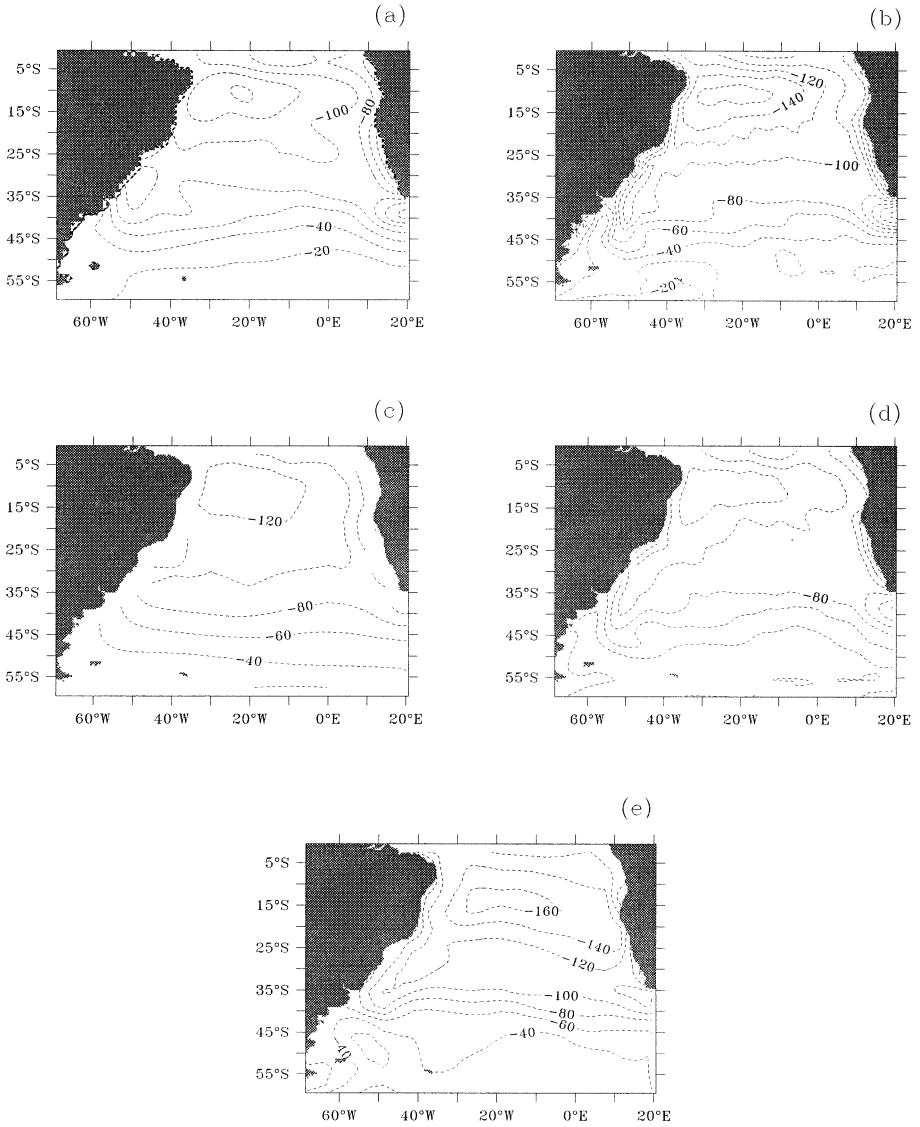

FIG. 3. South Atlantic latent heat net flux (W m^{-2}) annual mean climatology for (a) DaSilva, (b) NCEP, (c) EK, (d) SOC, and (e) NCAR CCSM model output. Contour interval is 20 W m^{-2}.

nor amount to the net ocean heat gain or loss in comparison with the latent heat. It is mostly directed from the atmosphere into the ocean except at high-latitude winters, when air–sea temperature contrasts become large enough that sensible heat loss becomes important.

The net heat flux (Fig. 4) is only shown here for the observed products because the net radiation components for the NCAR CCSM were not available. Work is under way to retrieve these components. Common characteristics are the heat gain band centered over the equatorial undercurrent, off the southwestern coast of Africa and adjacent to the southeastern coast of South America, south of about 35°S, associated with the southward penetration of the Malvinas Current.

In the Agulhas retroflection region, at approximately 45°S, 20°E, the ocean loses energy in all the climatologies, reaching in some products up to 100 W m^{-2} (Fig. 4a). This loss can be explained by the shortwave component systematic reduction caused by the cloud formation intensification over the region due to the colder westerly winds flowing over the warmer Agulhas Current waters in the area.

The DaSilva (Fig. 4a) and NCEP (Fig. 4b) climatologies show the other two places with net heat loss: the Brazil Current system at the western boundary, and the region, around 10°S, associated with the warm South Equatorial Countercurrent (SECC). The SOC climatology, however, presents a heat *gain* in the SECC region. But even the DaSilva and NCEP climatologies exhibit a significant difference in the net heat spatial pattern near the SECC region. In DaSilva, the heat loss band is confined between 10° and 20°S east of 20°W while

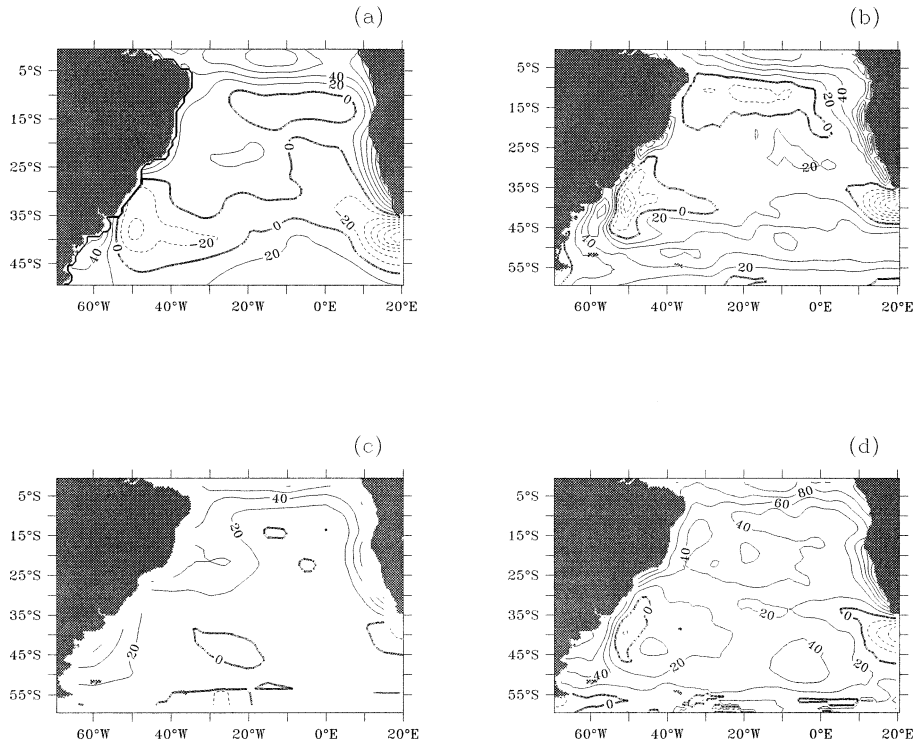

FIG. 4. South Atlantic net heat net flux (W m^{-2}) annual mean climatology for (a) DaSilva, (b) NCEP, (c) EK, and (d) SOC. Contour interval is 20 W m^{-2}.

the NCEP net heat loss is mostly confined to the western part of the domain, although the band extends all the way to the Greenwich meridian. In latitude it advances farther south, extending from 10° to about 25°S. It is also interesting to note that the heat loss region associated with the Brazil Current is confined to the western boundary in the NCEP (Fig. 4b) and SOC (Fig. 4d) climatologies, while in DaSilva (Fig. 4a) this region extends across the basin blending with the Agulhas Current net heat flux loss region.

The EK climatology (Fig. 4c) captures only minimum spatial features compared to the other data products, likely because of the lack of available data, specifically away from the continents. This climatology does not show the significant heat loss region associated with the Brazil Current in the western boundary. Quite the contrary, in the BMC region one notices a significant heat gain that extends erroneously northward, along the coast of Brazil. Furthermore, regions of heat loss in the SECC region and in the Agulhas Current region are barely discernible.

b. Mean seasonal cycle at specific locations

To better quantify the differences appointed in the previous section, time series at three specific sites corresponding to the regions with the largest variability are examined with respect to the seasonal cycle. The chosen points are at 40°S, 50°W (within the BMC region), 10°S, 10°E (off the African coast, within the upwelling system), and at 40°S, 10°E (where the Agulhas Current veers into the Atlantic Ocean). The seasonal cycle for the averaged latent, sensible, and net heat fluxes can be seen in Fig. 5 for all the observed products and NCAR CCSM simulation results.

The latent heat flux for the three locations is shown in Figs. 5a–c. All climatologies show very different behavior although SOC, DaSilva, NCEP, and EK present maximum values near the same time of the year (August) in the upwelling region off Africa, at 10°S, 10°E (Fig. 5a). The semiannual behavior of the SOC is present with a strong secondary maximum of -100 W m^{-2} observed in April. The largest phase difference occurs between NCAR CCSM and SOC. The NCAR CCSM product shows a minimum value in June and it presents two periods of maximum values in April and October. Comparatively, the largest latent heat loss is obtained by NCAR CCSM and the lowest by EK climatology.

In the southeastern Atlantic (Fig. 5b), all the time series show a large discrepant behavior. In this area, the largest latent heat loss is again obtained by NCAR CCSM and the lowest by NCEP. Because of the already known cold bias in this region and the associated increase in air–sea temperature differences, NCAR CCSM latent heat flux (Figs. 5a,b) is considerably larger.

The BMC region (Fig. 5c) shows a similar behavior (albeit large differences in magnitude) for all climatologies where the differences between the observations

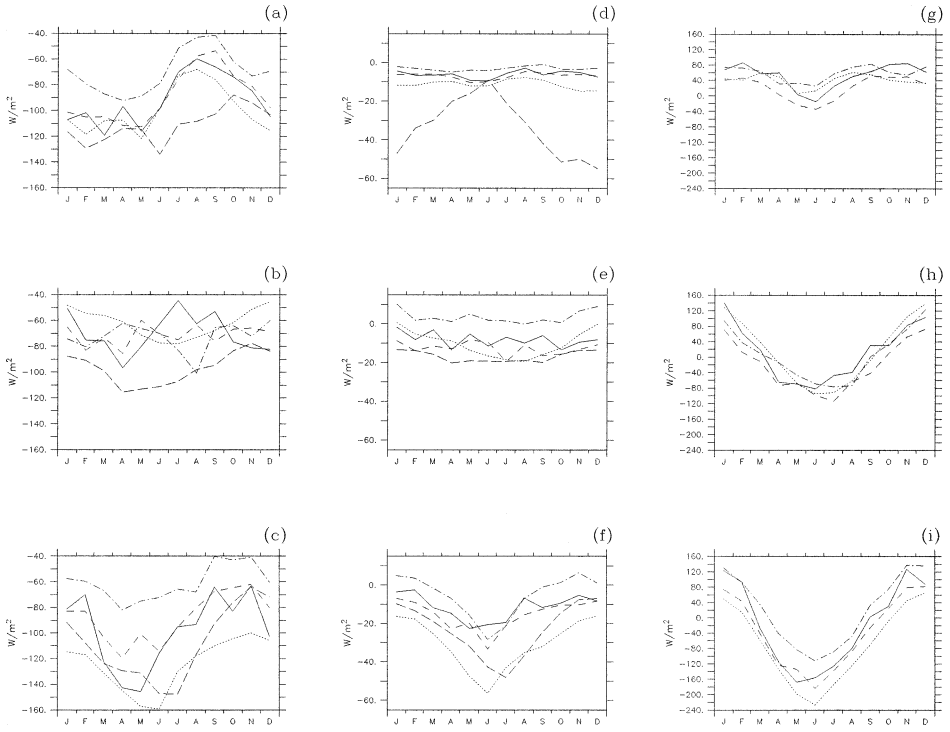

FIG. 5. Latent heat flux (W m^{-2}): (a) at 10°S, 10°E; (b) at 40°S, 10°E; (c) at 40°S, 50°W. Sensible heat flux (W m^{-2}): (d) at 10°S, 10°E; (e) at 40°S, 10°E; (f) at 40°S, 50°W. Net heat flux (W m^{-2}): (g) at 10°S, 10°E; (h) at 40°S, 10°E; (i) at 40°S, 50°W. Black line corresponds to SOC, dashed line to DaSilva, dotted line to NCEP, dashed–dot to EK. The long-dashed line corresponds to the NCAR CCSM, which is only shown for the latent and sensible heat fluxes.

are comparable to the difference between them and the NCAR CCSM. The seasonal cycle is pronounced with minimum values of latent heat during austral winter and maximum values in the summer. In this area, the largest latent heat loss is obtained by NCEP and the lowest by the EK time series.

Looking at the sensible heat flux at the three locations (Figs. 5d–f) it can be seen that the model does not capture either the magnitude nor the expected seasonal variability in the eastern Atlantic location (10°S, 10°E). This is also a known bias of the model. The meridional component of the wind stress in the NCAR CCSM (Wainer et al. 2000) is stronger, in particular between 20°W and 15°E where differences are of the order of 0.03 N m^{-2}. The global annual-mean NCAR CCSM wind stress is also stronger compared to the NCEP reanalysis product (Danabasoglu 1998). Therefore the model does not accurately represent the eastern Atlantic large-scale subsidence over the cool upwelled waters leading to the formation of low-level stratus decks and minimal precipitation, and thus the large discrepancy in the sensible heat flux, during the austral summer (Fig. 5d). There are differences between the climatological products themselves in this region (Fig. 5d), with NCEP presenting the largest magnitudes around -13 W m^{-2}, and EK the lowest, nearly -1 W m^{-2} that, although small, is consistent with the results of Bunker (1988).

The sensible heat flux for the Agulhas (Fig. 5e) and the BMC (Fig. 5f) locations presents differences between the climatologies themselves of the same order as the difference between the NCAR CCSM and the observations, although the NCAR CCSM presents the highest magnitudes during the austral summer months. In the southeastern Atlantic region (Fig. 5e), EK presents, during the whole year, a sensible heat flux from the atmosphere to the ocean. On the other hand, the other products indicate a systematic flux from the ocean to the atmosphere during the whole year with the NCAR CCSM presenting the largest loss.

The sensible heat flux is well behaved with respect to the seasonal cycle in the BMC region (Fig. 5f) with all climatologies presenting minimum values during austral winter. However, there is a lag of one month between NCEP (peaks in June, -55 W m^{-2}) and the NCAR CCSM (peaks in July, -48 W m^{-2}). DaSilva and EK present lower values and are slightly out of phase relative to the others (they peak in late June, approximately -38 W m^{-2}). The SOC seasonal cycle stands out by presenting a semiannual character with a secondary peak in August.

Despite the large discrepancies found for the latent and sensible heat fluxes, the net heat flux shows little discrepancy among the climatologies in their annual march with net heat gain in the austral summer and loss

in the winter. These little discrepancies indicate compensation between the sensible and latent heat fluxes.

4. Discussion and conclusions

The ocean responds most directly and rapidly to the atmosphere through the air–sea fluxes of heat, mass, and momentum at the surface. One of the greatest difficulties in the study of the South Atlantic is the lack of in situ measurements with time and space resolution adequate to validate the present estimates of these fluxes.

The estimates of the fluxes are strongly dependent on SST. The SST annual means investigated in this work showed that the differences between the climatologies (DaSilva, NCEP, EK, and NCAR CCSM) are prominent near the South American coast, in the BMC region, where the associated SST front is barely visible in the DaSilva dataset and NCAR CCSM model output, nonexistent in EK, but well represented in NCEP.

In this work we have also done an intercomparison of the annual mean and seasonal cycle for the South Atlantic fluxes of sensible, latent, and net heat for four observation-based products (DaSilva, NCEP, EK, and SOC) and the simulation results of the NCAR CCSM. The key regions of the BMC, Agulhas retroflection, and Benguela upwelling region off Africa were chosen for a closer examination of the fluxes. All climatologies show very different behavior. The SOC product presents sudden changes in the seasonal cycle evolution, departing from the more annual or semiannual-observed pattern of EK and NCEP. The EK shows comparable temporal behavior but different magnitudes possibly because this climatology covers a period where much less data were available.

It was found that the eastern Atlantic shows more differences among the climatologies than the BMC region in the west. It is also in the eastern Atlantic that the difference between NCAR CCSM results and observations are bigger, probably due to the lack of representation of stratus clouds that affect the air–sea interaction dynamics.

Boville and Jurrel (1998) show that over much of the globe, the SST errors are less than 1 K, even in the equatorial Pacific, where recent analyses suggest that the Shea et al. (1990, hereafter STR) estimate of climatological SST is 1 K too warm (see Reynolds and Smith 1994). The marine stratus regions off the western coasts of North and South America and off Africa are too warm by 2–3 K, resulting from a bias in cloud simulation in CCM3.

According to Norris and Weaver (2001) the atmospheric component of the NCAR CCSM overestimates shortwave and longwave cloud radiative forcing when vertical motion is upward (negative omega) and underestimates shortwave and longwave cloud radiative forcing compared to observations when vertical motion is downward. The model underestimates the all-sky liquid water path compared to observations when vertical motion is downward. These differences result from overproduction of frontal cloudiness during conditions of synoptic ascent and underproduction of low-level cloudiness during conditions of synoptic subsidence. Overproduction of cloudiness during ascent is caused by not representing subgrid variability in vertical motion. Underproduction of cloudiness during subsidence is caused by not representing boundary layer processes associated with stratocumulus.

In the BMC region, the differences between the NCAR CCSM and the observed datasets are comparable to the difference between the observations themselves.

The climatological products examined in this work have yielded notably different flux estimates probably because of uncertainties in exchange formulas, scarcity and poor quality of the observations, and different philosophies of data treatment. Direct flux measurements over the ocean are now possible locally but are difficult, very expensive, and rarely done. The more common bulk formula estimates of the fluxes, either based on observations of mean quantities or the output of numerical weather prediction (NWP) models, have uncertainties that are large compared to climate-related signals.

It was recognized already (see Taylor 2000) that accurate flux data are difficult to obtain. In general there is a trade-off between accuracy and temporal and spatial coverage. Furthermore, the same report gives detailed explanation of why the climatologies are different. As an example, it is stated that voluntary observing ships (VOS) derived fluxes [like Josey et al. (1999) and Da Silva et al. (1994)], tend to show more heat going into the ocean than what would be expected in the real world. Furthermore, in this specific work, the observation-based products used were derived from bulk formulas that are not all the same (including different exchange coefficients). A comprehensive intercomparison analysis was done by Zeng et al. (1998). Using six different flux algorithms on the Tropical Ocean Global Atmosphere Coupled Ocean–Atmosphere Response Experiment (TOGA COARE) ship data and Pacific TAO buoy data, they show that heat and momentum fluxes obtained differ significantly among the algorithms, under both very weak and very strong wind conditions, but agree with each other under moderate wind conditions. Algorithm results agree better for wind stress than for heat fluxes.

Key issues with regard to the fluxes analyzed in this work are their validity and their use in ocean models. Validation still requires systematic comparisons. Furthemore, models still have difficulty representing some of the air–sea-related dinamical processes which means that observed data improvement has to go hand in hand with model development. To validate coupled model results against observations is a significant and necessary endeavour. Agreement of a coupled general circulation model with observations is considerably more difficult to achieve than with an ocean model alone

forced by observations. The next step is to explore to what extent the South Atlantic upper-ocean heat budget, in particular at the BMC region, is dominated by surface heat fluxes, horizontal advection, upwelling, and entrainment.

Acknowledgments. This work was supported in part by Grants FAPESP-00/02958-7, CNPq 300223/93-5, CNPq 300561/91-1, and CNPq 300040/94-6. I. W. thanks Steve Hankin and the FERRET support group for the graphics. Also, I. W. thanks the National Science Foundation Small Grants for Exploratory Research program for supporting her visit to NCAR.

REFERENCES

Bèranger, B. B., K. Viau, E. Garnier, J. Molines, and L. Siefridt, 1999: An atlas of climatic estimates of air-sea fluxes. Equipe de Modèlisation des Ecoulements Océaniques de Moyenne et Grand Echelle, Tech. Report, LEGI, Grenoble, France, 82 pp.

Berliand, M. E., and T. G. Berliand, 1952: Determining the net longwave radiation of the earth with consideration of the effect of cloudiness (in Russian). Tech. Rep. 1, Izvestiya Akademii Nauk SSSR, Seriya Geofizicheskaya.

Boville, B., and P. R. Gent, 1998: The NCAR Climate System Model, version one. *J. Climate,* **11,** 1115–1130.

——, and J. Jurrel, 1998: A comparison of the atmospheric circulations simulated by the CCM3 and CSM1. *J. Climate,* **11,** 1327–1341.

Budyko, M. I., Ed., 1963: *Atlas of Heat Balance of the Earth.* Akad. Nauk SSSR, Prezidum. Mezhduvedomstvennyi Geofiz. Komitet, 69 pp.

Bunker, A. F., 1988: Surface energy fluxes of the South Atlantic Ocean. *Mon. Wea. Rev.,* **116,** 809–823.

Campos, E., and Coauthors, 1999: The South Atlantic and climate. *Proc. OCEANOBS'99: The Ocean Observing System for Climate,* Vol. 1, Saint Raphael, France, Cent. Nat. Etudes Spatiales.

Chelton, D., M. Schlax, D. Witter, and J. Richman, 1990: Geosat altimeter observations of the surface circulation of the southern oceans. *J. Geophys. Res.,* **95,** 17 877–17 903.

Cheney, R., J. Marsh, and B. D. Beckley, 1983: Global mesoscale variability from collinear tracks of seasat altimetry data. *J. Geophys. Res.,* **88,** 4343–4351.

Clark, N. E., L. Eber, R. M. Laurs, J. A. Renner, and J. F. T. Saur, 1974: Heat exchange between ocean and atmosphere in the eastern North Pacific for 1966–71. NOAA Tech. Rep. NMFS SSRF-682, U.S. Dept. of Commerce, Washington, DC, 108 pp.

Danabasoglu, G., 1998: On the wind-driven circulation of the uncoupled and coupled NCAR climate system ocean model. *J. Climate,* **11,** 1442–1454.

Da Silva, A., A. Young, and S. Levitus, 1994: *Algorithms and Procedures.* Vol. 1, *Atlas of Surface Marine Data 1994,* NOAA Atlas NESDIS 6.

Diaz, A. F., C. D. Studzinski, and C. R. Mechoso, 1998: Relationships between precipitation anomalies in Uruguay and southern Brazil and sea surface temperature in the Pacific and Atlantic Oceans. *J. Climate,* **11,** 251–271.

Esbensen, S., and Y. Kushnir, 1981: The heat budget of the global ocean: An atlas based on estimates from surface marine observations. Oregon State University, Tech. Rep. 29, 27 pp. plus figures.

Gordon, A., 1988: Brazil–Malvinas confluence. *Deep-Sea Res.,* **36A,** 359–384.

Josey, S. A., E. C. Kent, and P. Taylor, 1999: New insights into the ocean heat budget closure problem from analysis of the SOC air–sea flux climatology. *J. Climate,* **12,** 2856–2880.

Kalnay, E., K. C. Mo, and J. Paegle, 1986: Large amplitude, short-scale stationary Rossby waves in the Southern Hemisphere: Observations and mechanistic experiments to determine their origin. *J. Atmos. Sci.,* **43,** 252–275.

Large, W. G., and S. Pond, 1982: Sensible and latent heat flux measurements over the ocean. *J. Phys. Oceanogr.,* **12,** 464–482.

Lindau, R., 1995: A new Beaufort equivalent scale. *Proc. Int. COADS Winds Workshop,* Kiel, Germany, Institut fur Meereskunde Kiel and NOAA, 232–252.

Liu, W. T., K. B. Katsaros, and J. A.. Businger, 1979: Bulk parameterization of air–sea exchange of heat and water vapor including molecular constraints at the interface. *J. Atmos. Sci.,* **36,** 1722–1735.

Lutjeharms, J., and R. van Ballegooyen, 1988: The retroflection of the Agulhas Current. *J. Phys. Oceanogr.,* **18,** 1570–1583.

Norris, J. R., and C. P. Weaver, 2001: Improved techniques for evaluating GCM cloudiness applied to the NCAR CCM3. *J. Climate,* **14,** 2540–2550.

Olson, D., and R. Evans, 1986: Rings of the Agulhas Current. *Deep-Sea Res.,* **33A,** 27–42.

——, G. P. Podesta, R. H. Evans, and O. B. Brown, 1988: Temporal variations in the separation of brazil and Malvinas. *Deep-Sea Res.,* **35A,** 1971–1990.

Reed, R. K., 1977: On estimating insolation over the ocean. *J. Phys. Oceanogr.,* **7,** 482–485.

Reynolds, R. W., and T. M. Smith, 1994: Improved global sea surface temperature analyses using optimum interpolation. *J. Climate,* **7,** 929–948.

Rosati, A., and K. Miyakoda, 1988: A general circulation model for upper ocean simulation. *J. Phys. Oceanogr.,* **18,** 1601–1626.

Shea, D. J., K. E. Trenberth, and R. W. Reynolds, 1990: A global monthly sea surface temperature climatology. NCAR Tech. Note NCAR/TN-345, 167 pp.

Smith, S. R., 1988: Coefficients for sea surface wind stress, heat flux, and wind profiles as a function of wind speed and temperature. *J. Geophys. Res.,* **93,** 15 467–15 472.

Taylor, P. K., Ed., 2000: Intercomparison and validation of ocean–atmosphere energy flux fields. WCRP/SCOR Working Group on Air–Sea Fluxes, Final Rep. WCRP-112, WMO/TD-1036, 305 pp.

Wainer, I., P. R. Gent, and G. Goni, 2000: The annual cycle of the Brazil-Malvinas confluence region in the NCAR Climate System Model. *J. Geophys. Res.,* **105,** 26 176–26 178.

WMO, 1970: The Beaufort scale of wind force (technical and operational aspects). WMO Rep. 3, World Meteorological Organization Reports on Marine Affairs, 22 pp.

Zavialov, P., I. Wainer, and J. Absy, 1999: Interdecadal, interannual and seasonal variability off southern Brazil and Uruguay as revealed from historical data since 1854. *J. Geophys. Res.,* **104,** 21 021–21 032.

Zeng, X., M. Zhao, and R. Dickinson, 1998: Intercomparison of bulk aerodynamic algorithms for the computation of sea surface fluxes using the TOGA COARE and TAO data. *J. Climate,* **11,** 2628–2644.